

Structural color produced by a three-dimensional photonic polycrystal in the scales of a longhorn beetle: *Pseudomyagrus waterhousei* (Coleoptera: Cerambycidae)

Priscilla Simonis* and Jean Pol Vigneron

Research Center in Physics of Matter and Radiation (PMR), University of Namur (FUNDP), 61 rue de Bruxelles, B-5000 Namur Belgium
(Received 20 September 2010; revised manuscript received 5 November 2010; published 18 January 2011)

The cuticle of the longhorn beetle *Pseudomyagrus waterhousei* shows a diffuse pattern of mixed blue and violet colors. These colorations arise from a dense layer of droplet-shaped scales covering the dorsal parts of the cuticle. In spite of their lack of iridescence, these colors are shown to be structural and produced by an aggregate of internally ordered photonic-crystal grains. Computer simulations confirm that the blue and violet colors are caused by face-centered-cubic crystallites which dominantly expose their (111) surface to illumination and viewing.

DOI: [10.1103/PhysRevE.83.011908](https://doi.org/10.1103/PhysRevE.83.011908)

PACS number(s): 42.66.-p, 42.70.Qs, 42.81.Qb

I. INTRODUCTION

Three-dimensional photonic crystals have been found in a few groups of insects [1,2], essentially butterflies [3] and weevils [4]. Since the pioneering works that revealed their existence, much attention has been paid to these natural photonic structures [5], which recently appeared to be much more complex than initially understood [1]. In nature, photonic crystals serve the purpose of bringing coloration for signaling or camouflage. They help achieve an extremely wide variety of visual effects with a very limited number of materials. Very often, however, the structures responsible for light control also contribute to other properties, such as thermal control or hydrophobicity [6]. As a consequence, natural geometrical structures tend to increase in complexity: Understanding the purpose of submicron structures in living organisms inherently calls for multiscale, multifunctional, and multiphysics arguments.

Natural and artificial photonic-crystals studies follow different, complementary roads. Works on natural photonic crystals tend to focus on the way a light flux is controlled by a complex, multiscale structure, while the field of artificial photonic crystals mainly puts the emphasis on how to produce materials with low-loss evanescent waves, appropriate to localize and guide photons.

Face-centered cubic structures have been identified in the scales that cover some coleopters and, in particular, on weevils. The structure discovered there has sometimes been compared to opal [4], inverse opal (see p. 158 of Ref. [7]; see also Refs. [8–10]), a scaled analog of atomic diamond [11], or a stack of corrugated sheets [12]. In this latter work, the coloring structure—providing a noniridescent structural orange—has been identified as a photonic polycrystal, the crystallites (grains, or domains) being internally organized in a face-centered cubic symmetry. In the case of weevils, the small number of identified structures would not be able to produce the large variety of visual effects observed in the absence of long-range disorder. This calls for the examination of many more examples, to be found in the Curculionidae (i.e., weevils) family or elsewhere.

One systematic procedure to explore biodiversity in search of new three-dimensional structures is to collect data on species, genera, or families of insects close to the weevils in order to maximize the chances of finding sister pairs where similar constructions have taken place. This procedure has driven us to the brightly colored beetle shown in Fig. 1. This particular insect gets its blue coloration from a three-dimensional structure based on a photonic polycrystal similar to those found in weevils.

Because of the way living organisms' evolution has developed, a systematic search for the occurrence of a relevant structure can start with the examination of the local branches of a phylogenetic tree, in search of species pairs that share not too distant common ancestors. Biologists know how to determine the distance between species. The ideal—time-consuming and expensive—approach requires fully deciphering the ordered contents of every gene of both species (or, more economically, a few choice genes), targeting the number of mutations needed to produce those sequences from a common ancestors genome. The classification follows from a combinatorial calculation which targets the most probable tree. Another short-cut rests on the hybridization of DNA, where the bonding force between one strand of DNA from one species and a complementary strand from the other species measures the number of mismatches, hence the “distance” between the species. To split a perfectly matched DNA, 85 °C is enough, while a lower temperature is expected for hybridized DNA from distant species (cooling down by 1 °C indicates about 1% more mismatch).

The classification of species for the purpose of naming, for plants and for all other kingdoms alike, also follows a hierarchical scheme: “subtypes” are nested under “super-types” so that grouped subtypes inherit the same general traits as the supertypes in which they belong, but can be differentiated from each other by additional specific properties. This “taxonomical” arrangement happens to be applicable to the classification of living organisms and can be used as a basis for the precise, scientific naming of all species. The history of evolving species is, of course, behind this successful way of classifying all life on Earth. Each living individual—animals, plants, fungi, and some others—are determined according to the kingdom, phylum, class, order and suborder, superfamily and family, genus, and species to which they belong. Species grouped under the same genus

*priscilla.simonis@fundp.ac.be



FIG. 1. (Color online) The bright blue longhorn beetle (*Pseudomyagrus waterhousei*) under investigation in the present paper. The blue coloration appears diffuse and lacks iridescence, but its origin is structural. (scale bar 1 cm).

name should be genetically closer than species which belong to a different genus. The same should also be true for species in the same family or species in the same superfamily, etc. The genetic distance can, to some large extent, be read in the taxonomic organization of living organisms, though evolution deals with the history of reproducing species, while taxonomy deals with the organization of the subset of observed (living or extinct) species.

Following this, a “tree of life” can be determined, describing the evolution path that led to the classification of living species [13]. Figure 2 shows the most plausible road to arrive at the group of insects belonging to the type “Cucujiformia.” This group includes the weevils where three-dimensional photonic crystals have been found. From this tree, it is easy to determine genetically close types of insects, with the hope that the same opportunities to develop similar photonic structures can appear. One very attractive group of insects in this position is the family of Cerambycidae (the “longhorn beetles”), with more than 20 000 species described. They can usually be recognized by their very long antennae, used for sensing. Many of these beetles are considered a serious pest by humans, since their larvae bore into wood, where they cause extensive damage. These insects often show a cryptic appearance, but brightly colored species can also be found. Similar to weevils, these colored longhorns have often developed scales attached to specific areas of the cuticle surface. This suggests a potentially large diversity of coloring structures.

Among all these beetles, the Malaysian longhorn *Pseudomyagrus waterhousei* (Gahan, 1888) is particularly interesting because of its bright blue coloration (see Fig. 1). In the present paper, we consider the origin of this bright but diffuse blue and develop the arguments to show that this visual effect is the result of the presence of a photonic polycrystal in the scales that cover most parts of the beetle’s cuticle.

The paper is organized as follows. Section II summarizes the optical properties of the blue areas on the beetle’s cuticle. Section III examines the morphology of the colored areas for lengths varying from a fraction of a millimeter to deep below the micron. Section IV analyzes the photonic structure revealed by scanning electron microscopy, in order to show that this structure is indeed responsible for the observed optical properties. Models for the photonic structures serve as a basis for simulations of the light backscattering. Incoherent

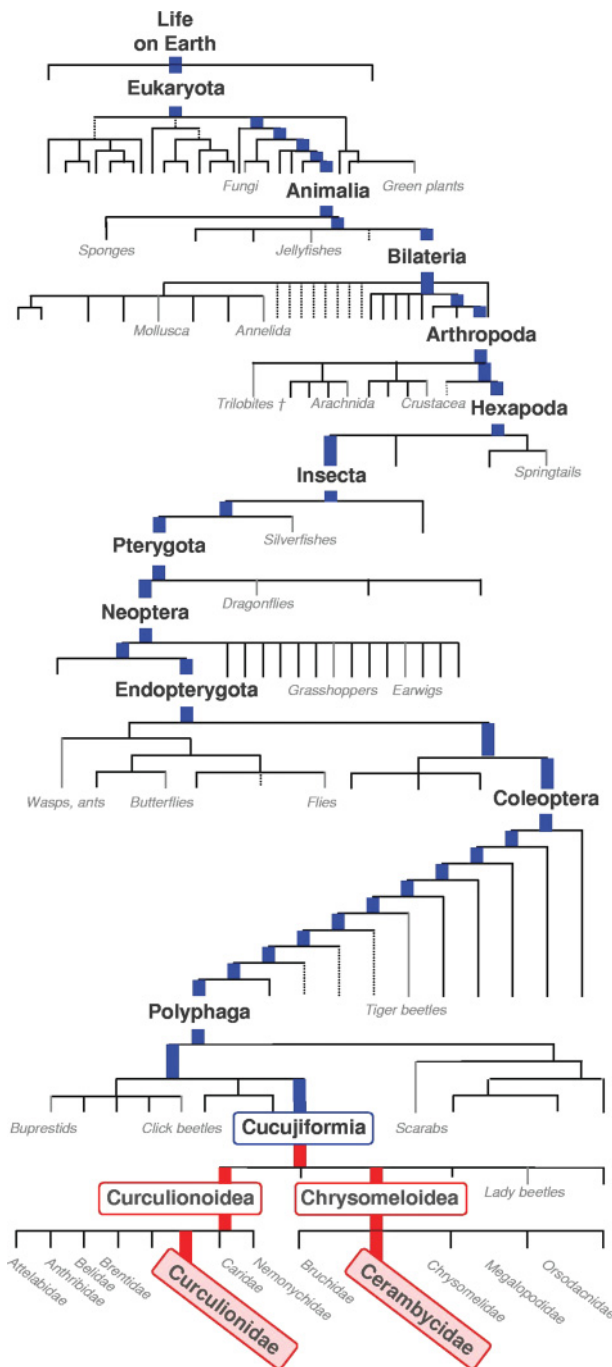


FIG. 2. (Color online) The road to weevils (Curculionidae) and longhorns (Cerambycidae), showing that these families of insects are close to each other [13] from a phylogenetic point of view. Some of the diverging branches toward other well-known types of insects are indicated for information (gray lettering).

scattering is introduced to explain the loss of iridescence in the far field. Section V draws conclusions for this work and addresses a few perspectives and consequences of the exposed results.

II. OPTICAL PROPERTIES

Pseudomyagrus waterhousei is a longhorn originating from the Malay Peninsula [14] and neighboring areas (Java,

Sumatra, Borneo, Nias Island) [15]. Little seems to be known about its biology.

This longhorn shows colors that can be described as dominantly blue and violet, except for a series of black dots. The violet regions seem to be larger on the male than on the female, a sexual dimorphic trait that adds to the different sizes of the body (larger in the female) and the length of the antennae (shorter in the female). Only female specimens have been analyzed for the purpose of the present discussion.

Several specimens of the longhorn were obtained from an insect collector. The area of the cuticle surface that was put aside for optical and morphological measurements is located on the large blue part of the *elytra* of the insect—the hard colored cases that protect the flying insect's wings.

For optical properties assessment, we used the outer surface of a large piece of an elytron, glued onto a microscope slide covered with white paper.

Visual inspection of the sample through a magnifier lens (10×) already makes clear that the cuticle is covered by small scales. The black dots, forming a marking pattern on the outside of the elytra, correspond to regions that lack scales and where the dark surface of the cuticle is directly apparent. These regions form small rectangular spots (see Fig. 1) visible to the naked eye. The use of a larger magnification, with a reflection mode optical microscope, reveals the precise shape of the scales. These appear as elongated droplets, with a grazing implantation, so that they cover the cuticle, lying flat on its surface. They are packed so that each one slightly overlaps its neighbors, all of them with their sharp tip oriented toward the end of the insect's abdomen (see Fig. 3). Individually, the reflection from each scale is very bright. A single scale produces several spots of various metallic colors, dominantly blue and violet, with yellow, pink, or green also marginally present. The incoherent mixing of all these reflections results in an average strongly desaturated bluish hue, which, from large distances, remains stable under any change of viewing direction.

It is interesting to note that the insect assumes a dull violet-blue color to the naked eye, while it shows a variety of different directional colors, when viewed in detail with the help of

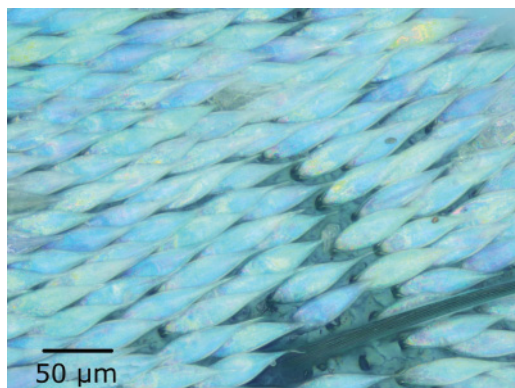


FIG. 3. (Color online) The cuticle of the *Pseudomyagrus waterhousei* is covered by drop-shaped scales. In an optical microscope, they show iridescence, with blue and violet colors much more frequent than pink, yellow or green. The image was taken with an Olympus BX61 optical microscope. The magnification in this picture is 60×.

an optical microscope. Incoherent mixing of random colored pixels that produce a dull coloration has already been identified in other insects, including butterfly wings [16].

In order to characterize more precisely the chromatic response of the scales, spectrophotometric measurements were performed with a double-beam spectrophotometer (Perkin Elmer Lambda 750S). This apparatus is equipped with an integrating sphere and prealigned tungsten-halogen and deuterium sources, covering the UV-visible and the near-infrared spectral regions. The integrating sphere gives access to the total hemispheric reflectance. The sample is placed on one of the poles of the sphere and the incident beam enters the sphere from the opposite pole, striking the sample at a fixed incidence angle of 4°. The collection of the specularly reflected beam can be suppressed, because of the presence of an closable “escaping” hole, in the specular direction.

The curves in Fig. 4 show the total hemispheric reflection factor (solid line) and the nonspecular diffuse scattering (dashed line) of the surface of the longhorn elytron. The measurements have been made in succession without moving the sample, addressing the same area of the cuticle in both measurements. The light beam was depolarized before reaching the sample. Obviously, the suppression of the specular beam brings literally no change to the global light scattering, suggesting that the structure is very effective in diffuse scattering, a fact, as observed, consistent with the lack of iridescence (see Fig. 1).

The spectrophotometric measurements shows the presence of a broad, but well-defined, peak located near 476 nm, with a nearly constant sideband starting near 328 nm. All wavelengths contribute to the spectrum through the presence of a nonzero background, leading to a further desaturation of the observed color. The sideband spans a range of wavelengths extending over more than 100 nm.

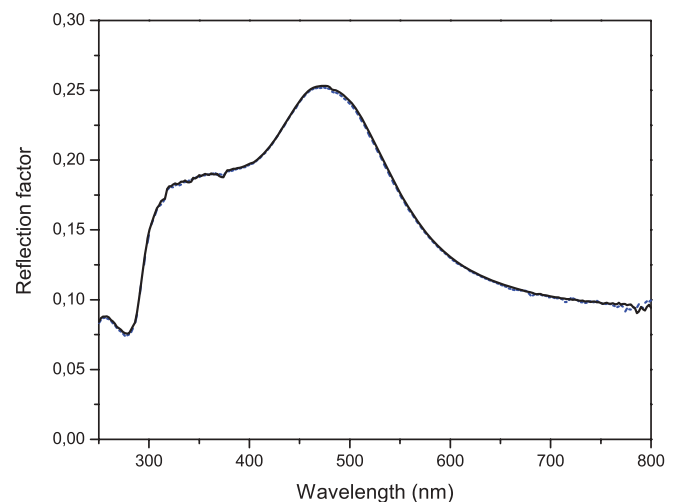


FIG. 4. (Color online) Total reflection factor of the cuticle (solid line) and out-specular reflection factor (dashed line) taken from the same area. An iridescent reflection is typically indicated by a difference between the results of these two measurements. In the case of the *Pseudomyagrus waterhousei*, there is no iridescence.

III. NANOMORPHOLOGY

Parts of the elytra removed from the longhorn body, similar to those used for optical measurements, were cut into small rectangular pieces, in liquid nitrogen at a temperature low enough to harden the chitinous material and increase the chances of a neat fracture of scales. Each of these pieces were pasted, using a conducting glue, on a metallic sample holder. The whole mount was metallized (20 nm of gold) to ease charge elimination and the prepared sample was introduced in a JEOL 7500F high-resolution field-effect scanning electron microscope.

The fractured scale appears to be composed of an external cortex wrapping a region filled with tiny chitin spherules. The outer surface of the cortex, facing out of the insect's body, shows an uneven surface, with parallel, longitudinal grooves, approximately $1\ \mu\text{m}$ apart. Each of the ribs protruding between the grooves also shows an uneven surface, wearing finer ribs, or "flutes," assuming an oblique orientation with respect to the grooves' direction. Viewed from the normal to the scale's surface, these flutes appear to be arranged in a kind of herringbone pattern. This hard and stiff cortex is about 500 nm thick. Inside the envelope formed by the solid cortex, small chitin spherules arrange themselves to form a regular pattern, as seen at the bottom of the scale in Fig. 5.

The spherules are close packed, touching each other without any noticeable spacer. The analysis of many scales has shown that their diameter is usually constant and can be estimated to be $212 \pm 21\ \text{nm}$. The distribution of diameters was obtained by sampling about a hundred spheres from a dozen broken scales. This direct-space approach is more appropriate for three-dimensional structures than Fourier transforms, which require perfect two-dimensional projections [17]. In each scale, the spherules are locally arranged into well-ordered crystallites, sometimes as small as $1\ \mu\text{m}$ in width (see Fig. 6, where the grain boundaries of some of the crystallites are suggested by black lines). The internal structure of the



FIG. 5. Electron microscope image of a broken scale randomly selected on one of the elytra of the longhorn *Pseudomyagrus waterhousei*. The scale has an external cortex filled with a regular arrangement of monodispersed chitin spherules. (scale bar 1 micron).

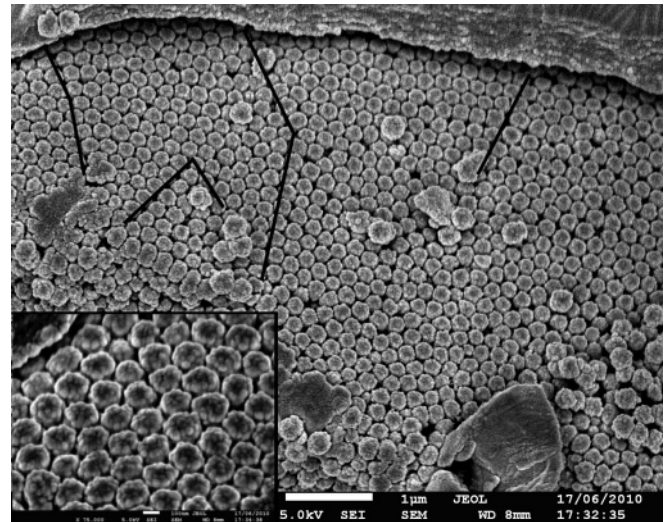


FIG. 6. The spherules inside a scale are arranged in grains assuming different orientations. Some of the grain boundaries are shown as solid lines. The spherules inside some crystallites appear to be arranged, in the fracture plane, at the sites of a triangular lattice, an arrangement consistent with the (111) orientation of a three-dimensional face-centered cubic lattice. In the inset, the diameter of the spherules can easily be measured and the larger resolution confirms that their connection to each nearest neighbor occurs through tangential contacts, with no sign of a solid spacer. (scale bar 1 micron).

scales appears, in the fracture, as a two-dimensional periodic arrangement of spheres: We often observe that the spheres occupy the sites of a triangular lattice, as shown in Fig. 6, and, on rare occasions, the sites of a square lattice, as presented in Fig. 7. These images (Figs. 6 and 7) are produced on scales fractured longitudinally, parallel to the cuticle surface. These observations, and many others, using different fracture plane orientations, strongly suggest that the spherules are locally distributed, in three dimensions, at the sites of a face-centered cubic lattice. The coherence of this organization is, however, limited to the volume of the grains, while the different grains are free to randomly assume a few specific orientations. The face-centered cubic structure generates the observation of a triangular lattice when the fracture occurs along a (111) reticular plane and a square lattice when the fracture coincides with a (100) reticular plane. The overall structure of the internal part of the scales can be described as a photonic polycrystal, a form of multiscale photonic structure characterized, simultaneously, by order for the short-range volume of the grains and disorder for the long-range granular distribution. The long-range disorder is related to the variation of the shape of the crystallites and the variations of their orientation.

A careful analysis of the occurrence frequency and the areas occupied by square and triangular surface lattices in the sampled scales provides an estimate of the relative importance of the (111) and (100) orientations in the polycrystalline structure. The (111) orientation is found to occur about 4 times more frequently than the (100) orientation. Assuming no other orientation (no encounter found), the weight of the (111) orientation appears, more precisely, to be 0.22 and the weight of (111) is 0.78.

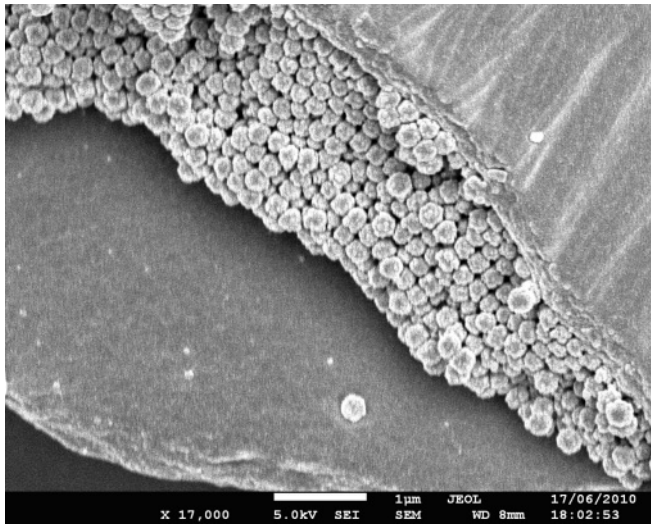


FIG. 7. A square structure of the spherules is also seen, sometimes, on the fracture plane occurring along the upper surface of the scales. This distribution of the spherules occurs along the (100) reticular plane of a three-dimensional face-centered cubic lattice. (scale bar 1 micron).

Scanning electron microscopy (SEM) offers the advantage over transmission electron microscopy (TEM) that the direction of viewing can be chosen *after* the scale has been prepared. Also, because the fracture follows the weakest cohesion surface, distortions of spherule aggregates are minimized. Compared to the thin planar slice needed for TEM, the irregular fracture offers many occasions to display three-dimensional details. These can be used to recognize the crystallographic arrangement, even if—as seen in the present study—the grains are very limited in size. For more coherent structures, as in butterflies [18,19], TEM does provide complementary, useful, information.

We based the analysis of the structure on a few randomly chosen scales, all of them showing the spherule organization that leads to the described blue-violet reflection. On very rare occasions, however, the grains observed under the optical microscope showed the occurrence of pale green, yellow, or pink colors.

Figure 8 shows a rather exceptional structure, where the granular structure of the medium filling a scale shows an amorphous region next to an ordered, polycrystalline, aggregate. The amorphous region appears to be developed from spheres with unequal diameters, ranging from 170 to 300 nm. The existence of diameters that exceed the average diameter in ordered regions (212 nm) suggests that the very desaturated colors that appear as green, yellow, or pink could be explained by the presence of such disordered grains (see modeling in what follows).

IV. MODELING

The model and simulations in this section intend to explain the desaturated blue color observed on the *Pseudomyagrus waterhousei*.

The face-centered cubic (fcc) lattice photonic structure, with a sphere diameter of 212 nm, has been considered for

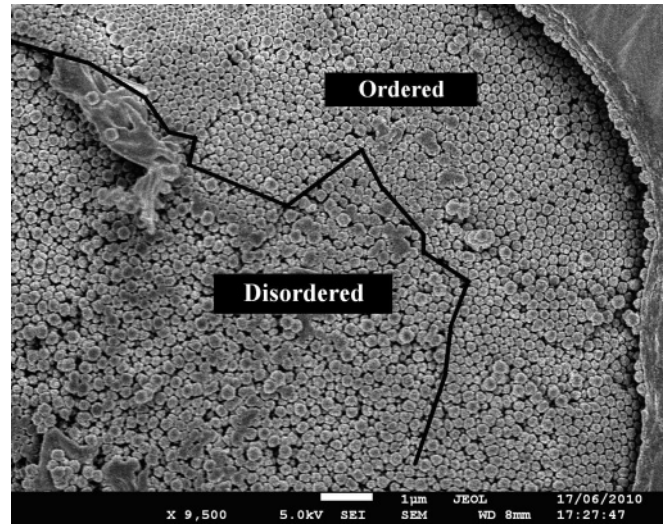


FIG. 8. A special—rather rare—scale, where ordered grains (with monodisperse spherules) and an amorphous region (with spherules of slightly varying diameters) coexist. (scale bar 1 micron).

two distinct orientations with, respectively, the (111) and (100) reticular planes parallel to the surface of the elytron. The spheres were assumed to be made of a homogeneous chitinous material, reduced to an isotropic, transparent and nondispersive medium ($n = 1.56$). The interstitial space is filled with air ($n = 1$). As observed in SEM images, the lattice parameter of the fcc structure is such that the spheres are in contact (cubic lattice parameter 293 nm).

Reflectivity spectra are calculated with three-dimensional transfer matrices [20], a computational technique designed to describe the interaction of the light with a photonic-crystal film. This technique allows for the calculation, at a fixed frequency, of the intensity of the beams diffracted back from a photonic-crystal film. Note that in this approach, the refractive index is *not* averaged laterally over periodic planes, so that the lateral inhomogeneity is fully accounted for. The periodic parts of the Bloch electromagnetic fields are expanded as a two-dimensional Fourier series for the direction parallel to the photonic-crystal film surface, while a direct-space representation is used in the direction of the normal. In agreement with experiment, the hemispheric reflectivity is calculated as a function of the incidence wavelength and the incidence angle.

In the present case, the photonic structure is more complex than a coherent photonic crystal because of long-range disorder. The response of a photonic polycrystal with orientational disorder is an important chapter in natural optics. The idea, already developed to explain noniridescent structural coloration in weevils [1,12], is that polycrystals can be viewed as a multiscale structure, where each grain produces reflected and transmitted diffracted beams which enter the next grain under a random incidence, before exiting, after multiple direction changes, under a direction largely decorrelated from the original incidence direction. Under a well-defined viewpoint, the light produced by a collection of small grains is the incoherent superposition of light beams originating from a wide range of incidences, with the consequence that the variation of color with the incidence angle is lost and the reflectance spectrum is significantly broadened. One

way to introduce these diffuse scattering mechanisms in the calculation of the film response is to average the reflected energy from all accessible configurations over all incidences (varying polar and azimuthal angles).

The hemispheric reflectivity is calculated for a photonic crystal film which stacks 32 layers [film thickness $9.6 \mu\text{m}$ for (100) orientation, $16.6 \mu\text{m}$ for (111), thick enough to represent infinity]. The spectral interval is somewhat wider than for the human visible range: from 250 to 800 nm. The light was unpolarized, as required to comply with experimental conditions (the reflectances for TE and TM polarization are calculated and averaged with equal weights). The incidence direction is spotted by a polar angle and an azimuthal angle. The average is carried out by sampling the directions with a resolution of 2° (from 0° to 90°) for polar angles and 10° (from 0° to 360°) for azimuths.

The result is shown in Fig. 9. The crystal orientation exposing a (111) surface shows an important peak located near 480 nm and a sideband at shorter wavelengths. This agrees with the experimental dominant reflection, found at 476 nm and with the sideband shown experimentally. The

(100) orientation shows a double peak appearing at 417 and 448 nm, as well as an increasing contribution in the UV part of the spectrum. This spectrum is only a minor correction to the reflected color because this orientation of the crystal is, as we have seen before, less frequent than (111).

At large distances, the responses from the orientational disorder superpose incoherently, due to the large distance between the grain centers. The resulting superposition, with 75% from the (111) orientation and 25% from (100) is shown on Fig. 9, with the label “0.25(100) + 0.75(111).” The weights were obtained by fitting the mixed calculated spectrum to the experimental data (“Exp” on Fig. 9, identical to Fig. 4) between 300 and 800 nm. The optimal weight [25% for the (100) orientation] agrees with the observed 22% reported in Sec. III. It is clear that the main blue peak should be associated with the dominant orientation (111) of the fcc crystal, lying flat on the cuticle surface. The side band, on the violet side, is already present in this dominant orientation. The next-most-frequent orientation, (100), does not contribute to the blue peak, but contains a contribution which can affect the sideband. The optical spectrum measured on the beetle elytron can then be essentially understood as arising from the (111) orientation of the photonic crystallites.

In order to appreciate the colorimetric quality of the color prediction (for the human view), we can calculate the chromatic coordinates on the CIE 1931 color space chromaticity diagram. This leads to the following results: for experiment, $x = 0.26$, $y = 0.30$ and for the calculated values, $x = 0.23$, $y = 0.30$. This result is shown in Fig. 10, where the two dots show the locations of these calculated and measured xy chromaticity coordinates.

The very desaturated green, yellow, and pink colors that occur at some rare points of the cuticle, when observed

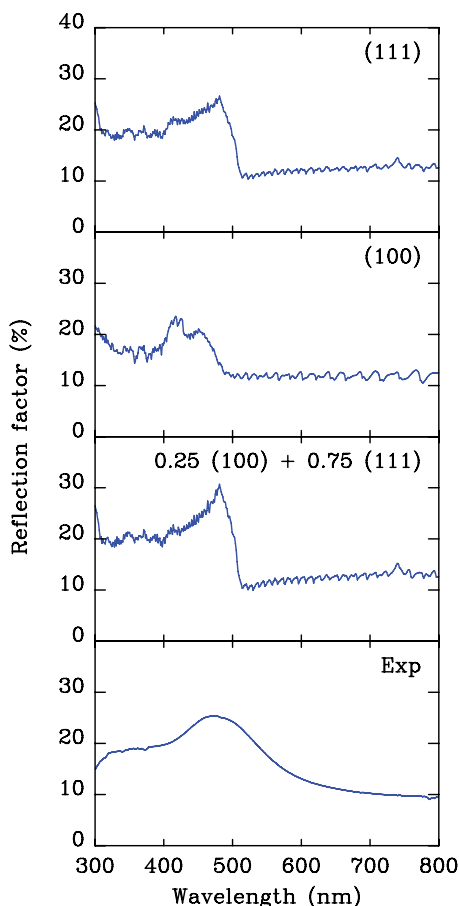


FIG. 9. (Color online) Theoretical simulation of the reflectance of a grain with the exposed surface aligned with the (111) and (100) reticular planes. The graph noted Exp is the experimental spectrum (see Fig. 4), reproduced for comparison. The spectrum labeled “0.25 (100) + 0.75 (111)” is an incoherent average of the preceding (100) and (111) spectra, best fitted to the experimental values. The resulting contribution of (100), 25%, agrees with the value 22% drawn from the SEM image analysis.

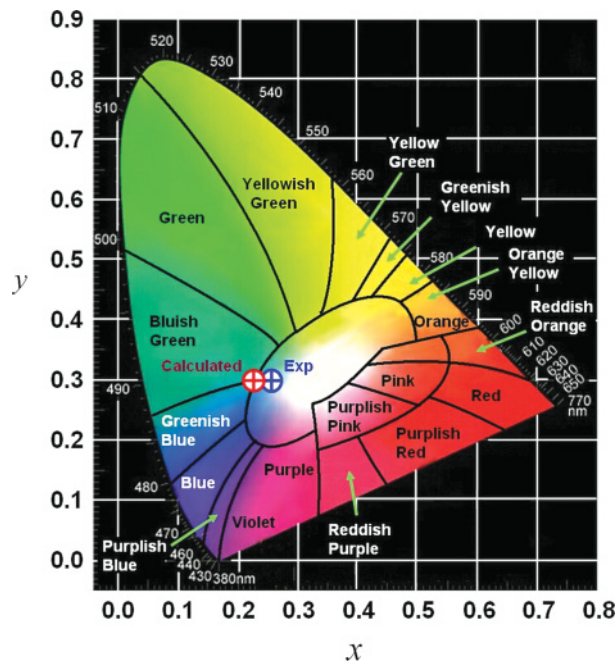


FIG. 10. (Color online) Calculated and measured chromaticity coordinates for a model which accounts for simultaneous (111) and (100) grain orientations.

TABLE I. Dominant reflected wavelengths for fcc structures with (111) surface for different sphere diameters. The sphere diameter in the blue-violet model is 212 nm, explaining the dominant color of *Pseudomyagrus waterhousei*.

Spherule diameter (nm)	Dominant reflected wavelength (nm)
180	407
200	453
212	480
220	498
240	543
260	588
280	634
300	679

through the optical microscope, can occur from grains with exceptionally large spherules appearing in a disordered grain. The observed diameters range, as described previously, from 170 to 300 nm. If we calculate the dominant color reflected for all spherule diameters in that range, assuming a (111) fcc structure, we obtain the calculated data presented in Table I. We can read the results in the following way: A green contribution (510 nm) arises from a spherule with a diameter close to 225 nm. For a yellow contribution (580 nm) a diameter of 260 nm is needed, while a red (pink) contribution (650 nm) requires a diameter of 290 nm. All these diameters have been occasionally observed on spherules in the disordered grains.

V. CONCLUSIONS

The discovery of three-dimensional photonic crystals in the scales of some weevils has opened the way to further discovery of natural photonic structures. At the start of the present work, a strong but heuristic hypothesis was made: The chances of finding similar (eventually differently evolved) photonic structures are better for insects that share not too distant common ancestors with weevils. Cerambycidae (longhorns) are a good example of these, with the advantage that this family is extremely large and has shown a wide variety of colorations and visual effects.

The Malaysian longhorn *Pseudomyagrus waterhousei* appears essentially blue and has scales. Its study, reported here, has been successful, in the sense that all scales are indeed structured, with a three-dimensional photonic polycrystal occupying the inside of a thin envelope forming a hard cortex. In the far field, the scales produce a diffuse scattering of white light, which is shown to be especially efficient in the blue (476 nm), with a violet sideband. At a larger scale, the scanning electron microscope reveals the presence of contiguous granular

domains, internally organized as a coherent arrangement of rigidly bound spherules. Each grain is a piece of photonic crystal built with spherules occupying the sites of a fcc Bravais lattice. Theoretical considerations suggest that the contents of the observed reflectance dominantly arise from photonic crystallites with (111) reticular plane parallel to the cuticle surface.

Natural three-dimensional photonic crystals can then be found in the large family of longhorn beetles. One interesting question which follows from this finding—and from the way the Cerambycidae family ended up to be chosen here—is whether the production of natural photonic crystals dates back to the common ancestors of weevils and longhorns, to be found in the infraorder Cucujiformia (plant-eating insects). As a warning to the reader, there is equally a good chance that the three-dimensional photonic crystals evolved *independently* in weevils and longhorns, so that the seemingly successful procedure suggested here for locating new structures may just have been a lucky guess. However, the other possibility is that, effectively, the genetic recipe for fabricating photonic crystals was already present in the common ancestors of these families of insects, so that there are deeper reasons to systematically explore the close cousins of our already known photonic-crystals producers. The oldest apparent fossil Cerambycidae appears to be *Cerambycomima* that has been found living in the late Jurassic, ca. 152 million years ago [21]. Since no further record of Cerambycid fossils exists in the Cretaceous period which follows Jurassic, this old insect is sometimes classified as a Chrysomelid, but it shares a number of traits with modern longhorns (long antennae and segmentation of the antennae with articulated flagellomeres). It may then be reasonable to estimate 152×10^6 years as the speciation date which leads to weevils and longhorns. At present, we do not know of *biological photonic crystals* that have been found in insects trapped in amber produced in this remote period. Nevertheless, it is interesting to note that Cucujiformia also contains a third prolific family of insects: Chrysomelidae. From this family, we know about 38 000 recent species, grouped under 2500 genera [22]. Coloration is very important for these insects and the coloration mechanisms in these Chrysomelids can be rather complex [23]. We speculate that this other large family could well be the next in which three-dimensional photonic crystals are ready to be observed.

ACKNOWLEDGMENTS

The authors acknowledge the use of Namur Interuniversity Scientific Computing Facility (Namur-ISCF). P.S. acknowledges the financial support of the Walloon Region of Belgium.

- [1] J.-P. Vigneron and P. Simonis, in *Advances in Insect Physiology*, edited by Jérôme Casas and Stephen J. Simpson (Academic Press, Burlington, 2010), Vol. 38, pp. 181–218.
 [2] S. Berthier, *Iridescences: The Physical Colors of Insects* (Springer, Heidelberg, 2006).
 [3] A. Argyros, S. Manos, M. C. J. Large, D. R. McKenzie, G. C. Cox, and D. M. Dwarthe, *Micron* **33**, 483 (2002).

- [4] A. R. Parker, V. L. Welch, D. Driver, and N. Martini, *Nature (London)* **426**, 786 (2003).
 [5] S. Kinoshita, *Structural Colors in the Realm of Nature* (World Scientific, Singapore, 2008).
 [6] S. Berthier, *Appl. Phys. A* **80**, 1397 (2005).
 [7] S. Berthier, *Iridescences: The Physical Colors of Insects* (Springer-Verlag, Berlin, 2006).

- [8] H. Ghiradella, *Ann. Entomol. Soc. Am.* **77**, 637 (1984).
- [9] V. L. Welch, in *Structural Colours in Biological Systems—Principles and Applications*, edited by S. Kinoshita and S. Yoshioka (Osaka University Press, Osaka, 2005).
- [10] A. Parker, in *SPIE Newsroom* (SPIE—The International Society for Optical Engineering, 2006).
- [11] J. W. Galusha, L. R. Richey, J. S. Gardner, J. N. Cha, and M. H. Bartl, *Phys. Rev. E* **77**, 050904 (2008).
- [12] V. Welch, V. Lousse, O. Deparis, A. Parker, and J. P. Vigneron, *Phys. Rev. E* **75**, 041919 (2007).
- [13] F. A. Bisby, Y. R. Roskov, T. M. Orrell, D. Nicolson, L. E. Paglinawan, N. Bailly, P. Kirk, T. Bourgoïn, and G. Baillargeon, *Species 2000 & ITIS Catalogue of Life: 2010 Annual Checklist* (Species 2000, Reading, UK, 2010); digital resource at [<http://www.catalogueoflife.org/annual-checklist/2010>].
- [14] K. Sakaguti, *Insects of the World 2, Southeast Asia II Including Australia* (Hoikusha, Osaka, 1981)
- [15] S. Breuning, *Nov. Entomol. (Paris)* **3**, 137 (1943).
- [16] K. Kertész, Z. Bálint, Z. Vértésy, G. I. Márk, V. Lousse, J. P. Vigneron, M. Rassart, and L. P. Biró, *Phys. Rev. E* **74**, 021922 (2006).
- [17] G. I. Márk, Z. Vértésy, K. Kertész, Z. Bálint, and L. P. Biró, *Phys. Rev. E* **80**, 051903 (2009).
- [18] P. Vukusic, J. Sambles, C. Lawrence, and R. Wootton, *Proc. R. Soc. London, Ser. B* **266**, 1403 (1999).
- [19] K. Kertész, Z. Bálint, Z. Vértésy, G. I. Márk, V. Lousse, J. P. Vigneron, M. Rassart, and L. P. Biró, *Phys. Rev. E* **74**, 021922 (2006).
- [20] J. Vigneron and V. Lousse, *Proc. SPIE* **6128**, 61281G (2006).
- [21] D. Grimaldi and M. S. Engel, *Evolution of the Insects* (Cambridge University Press, Cambridge, 2004), p. 393.
- [22] T. Seeno and J. Wilcox, *Leaf beetle genera (Col. Chrys.)* (Entomography Publications, Sacramento, CA, 1982), p. 221.
- [23] J. P. Vigneron, J. M. Pasteels, D. M. Windsor, Z. Vértésy, M. Rassart, T. Seldrum, J. Dumont, O. Deparis, V. Lousse, L. P. Biro, D. Ertz, and V. Welch, *Phys. Rev. E* **76**, 031907 (2007).